Observation of recoil magnetization curves outside the major loop in Co, Fe, and Ni films

J. Geshev [1,*] W. J. S. Garcia [2] V. Z. C. Paes [1] L. F. S. Azeredo [1] L. S. Dorneles [2] and A. M. H. de Andrade [1]

[1]*Instituto de Física, Universidade Federal do Rio Grande do Sul, Porto Alegre, 91501-970 Rio Grande do Sul, Brazil*

[2]*Departamento de Física, Universidade Federal de Santa Maria, Santa Maria, 97105-900 Rio Grande do Sul, Brazil*

(Received 17 May 2021; revised 12 August 2021; accepted 12 August 2021; published 25 August 2021)

We report a peculiar magnetization reversal observed in magnetron-sputtered Co, Fe, and Ni films. We found that some recoil (minor) magnetization curves lie entirely and way outside the major loop, a phenomenon referred to here as a *recoil-curve overshoot*. The greatly enhanced recoil curve's remanence and coercivity result in an up to 2.5-fold increase of loop's area. The model of pairs of exchange-coupled grains with misaligned anisotropy axes reproduces, in a very good agreement with the experiment, all key features of the recoil-curve overshoot as well as the kink that some major loops present before saturation. The disclosed features of the ferromagnetic hysteresis provide further insights into this important classical phenomenon.

DOI: 10.1103/PhysRevB.104.054436

I. INTRODUCTION

The most distinctive and intriguing phenomenon of ferromagnetism is the magnetic hysteresis. Practically all magnetism-based applications rely on particular aspects of hysteresis. From the theoretical point of view, magnetic hysteresis has attracted the interest of physicists and mathematicians concerning the comprehension of the involved physical mechanisms for more than a century.

Magnetization, M, vs magnetic field, H, hysteresis loop is the fingerprint of ferromagnetic materials [1]. One of its most important characteristics is the anisotropy field above which only reversible rotations occur. Its value depends, essentially, on the material's anisotropy and saturation magnetization, M_S. Major (or limiting, saturation) hysteresis loops are obtained for H cycled between fields greater in modulus than the anisotropy field. Otherwise, these are known as minor loops. Such a loop, obtained by starting from saturation and then reversing the field at a certain point (the recoil field) of the major loop, represents a recoil loop, which incorporates a first-order return branch [1] or, most popular, first-order-reversal curve, FORC. Minor loops might give information about the magnetic state and magnetization reversal processes [2]. For example, FORC diagrams represent a powerful tool to study reversal mechanisms and interparticle magnetic interactions [3]; the recently introduced δM_R plots [4] are also based on recoil-loop measurements.

To our knowledge, virtually any minor loop reported in the literature lies inside the respective major loop and covers an area smaller than the area of the major loop [5]. Here we report recoil curves, measured for Co, Fe, and Ni films with different types of intrinsic magnetocrystalline anisotropies, that lie entirely outside the major loop. Using a phenomenological model, we were able to reproduce this remarkable phenomenon and all key features of the corresponding major hysteresis loops.

II. EXPERIMENT

Polycrystalline Co films, with thickness between 5 and 150 nm, and 20- and 75-nm-thick Ni films were magnetron sputtered at room temperature onto either naturally oxidized Si(100) or onto 18-nm-thick Ta layers previously deposited on top of Si, covered with sufficiently thick protecting layers (Ta or Cr). Films with Cr layers deposited before Co appeared to be almost isotropic in-plane and did not present the phenomenon discussed below. A 25-nm-thick Fe film was also sputtered onto a glass substrate. In order to induce a uniaxial anisotropy, in-plane magnetic field of about 1.5 kOe was applied during deposition.

III. RESULTS AND DISCUSSIONS

In-plane magnetization curves were obtained at room temperature using three distinct techniques, namely, vibrating-sample magnetometry (VSM), alternating gradient-force magnetometry (AGFM), and magneto-optical Kerr effect (MOKE) magnetometry. The amplitude of the saturation magnetic field of 200 Oe used is sufficiently high to avoid minor-loop effects [6,7]. Details on the magnetization measurements are given in the Supplemental Material (SM). Hereafter, $\phi_H = 0^\circ$ refers to **H** parallel to the easy-magnetization axis, *EA*, where the coercive field, H_C, and saturation remanent magnetization, M_{RS}, are maxima. While major hysteresis loops are traced for H varied from $+200$ to -200 Oe and then back to $+200$ Oe, a recoil loop, $M_R(H)$, is measured as H is cycled between $+200$ Oe and a smaller (normally negative) field, called recoil field, H_R. Obviously, for H_R greater than the anisotropy field, the recoil loop presents the same characteristics as the major loop.

The x-ray diffraction spectra (not shown), obtained in Bragg-Brentano $\theta - 2\theta$ geometry and Cu $K\alpha$ radiation, show

*julian@if.ufrgs.br

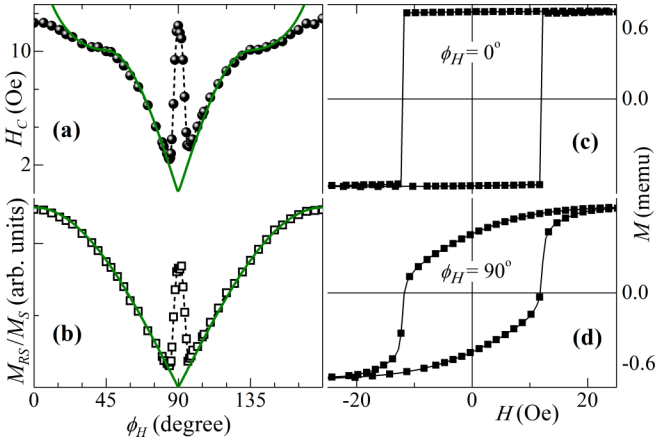

FIG. 1. Data obtained for the Ta/Co (20 nm)/Ta film via VSM. The symbols in (a) and (b) give $H_C(\phi_H)$ and $M_{RS}(\phi_H)$ and the solid lines correspond to coherent rotation. Major hysteresis loops measured for (c) $\phi_H = 0^\circ$ and (d) $\phi_H = 90^\circ$.

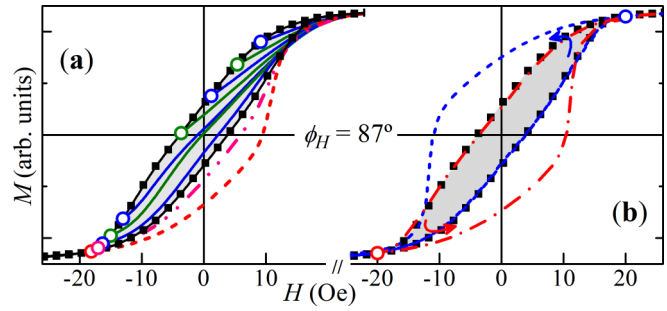

FIG. 2. Data obtained for $\phi_H = 87^\circ$ for the Ta/Co (20 nm)/Ta film. (a) Major loop and recoil curves with $|H_R| < 20$ Oe. Note that the dashed and dash-dotted curves lie outside the major loop, i.e., RCO. (b) Major loop (full symbols), where H is varied between -35 and $+35$ Oe, and recoil loops traced for H changed from $+35$ to -20 and back to $+35$ Oe (dash-dotted line), and from -35 to $+20$ and back to -35 Oe (short-dashed line). The open symbols give the starting points of the recoil curves.

that the Ta seed layer results in highly textured surfaces as expected [8]. The Ta/Ni films show an fcc (111) Ni textured phase; in the Ta/Co films, the observed peaks coming from Co fcc (111) and hcp (002) planes are very near to each other and overlap in a central broad peak. The rest of the films, grown on Si or glass substrates, did not show textured phases. From these data, the average grain size of our polycrystalline ferromagnetic films was estimated using the Scherrer formula. This size raises from approximately 4 to 17 nm as the Co thickness increases from 5 to 150 nm for the Ta/Co/Ta film series. The respective values for the 20- and 75-nm-thick Ni films are 16 and 31 nm.

Figure 1 gives the angular variations of H_C and M_{RS} of the major magnetization hysteresis loops for a 20-nm-thick Co film, together with those predicted by the uniaxial-anisotropy Stoner-Wohlfarth model [9]. There is an excellent agreement between theory and experiment for about two-thirds of the **H** orientations. The divergence near the *EA* is usually attributed to magnetization reversal governed by domain-wall motion. Here, this classical model does not fit in very close vicinity of 90° as well. The major loops obtained for $\phi_H = 0^\circ$ and 90° are plotted in Fig. 1. While the former is virtually rectangular, the loop measured for $\phi_H = 90^\circ$ is round in shape and presents lower M_{RS} but nearly the same H_C as the *EA* loop. This reflects in the very sharp peaks in $H_C(\phi_H)$ and $M_{RS}(\phi_H)$, centered at 90°. The same holds for the rest of our films, exemplified in Fig. S1 of the SM [10], for Ni and Fe films.

Such a distinct behavior has previously been observed for a number of materials (see, e.g., Ref. [11], and the references therein). Idigoras *et al.* [11,12] have attributed this phenomenon, referred to there as a collapse of the hard axis, to crystallographic disorder. This should also be the cause for the hard-axis collapse of our films which present, essentially, characteristics of the (induced during deposition) in-plane uniaxial magnetic anisotropy only.

To shed light on the magnetization reversal responsible for this intriguing feature, recoil-loop measurements were carried out. Major and recoil loops, obtained for $\phi_H = 87^\circ$ for the Ta/Co (20 nm)/Ta film, are shown in Fig. 2(a). The major loop is much more tilted than that obtained for $\phi_H = 90^\circ$ shown in Fig. 1(d), with rather lower values of H_C and M_{RS}. Remarkably, recoil curves with H_R in the vicinity of the apparent closure field (negative) lie well outside the major loop. This phenomenon will be further referred to as *recoil-curve overshoot* (RCO). None of the recoil curves measured for $\phi_H = 90^\circ$ and for $\phi_H < 65^\circ$ show such a peculiar behavior.

In Fig. 2(b), the representative major loop is traced using a maximum field's amplitude of 35 Oe (sufficient for saturation). The H_R values of the two recoil loops are $+20$ or -20 Oe, depending on the sign of the starting saturation field. These loops, with H_C and M_{RS} much greater than the major loop's ones, are symmetric through the origin and show significant RCO.

The RCO manifestation was further verified and undoubtedly observed in all films of the Ta/Co and Si/Co series. Representative Ta/Co data are presented in Figs. 3(a) and 3(b), and results for Si/Co films are given in Figs. 3(c) and 3(d). The cap-layer material does not impact qualitatively on the RCO.

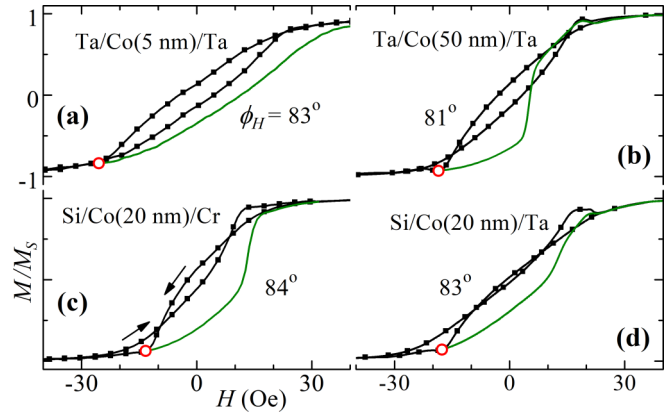

FIG. 3. Representative major loops (symbols) and recoil curves (lines) showing RCO, obtained via VSM for Co films with different thickness and/or cap layers, deposited on either Ta or Si substrates. The open symbols give the starting points of the recoil curves.

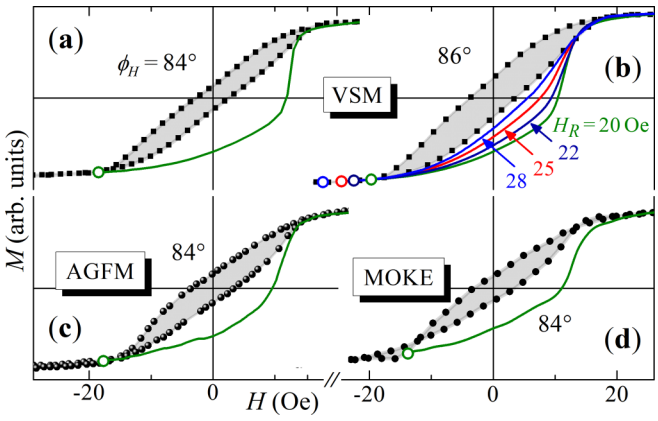

FIG. 4. (a) Major loop (symbols) and a recoil curve (solid line), obtained via VSM for the Ta/Co (20 nm)/Ta film for $\phi_H = 84°$. (b) Major loop (symbols) and recoil curves (lines) with $|H_R| \geqslant 20$ Oe, measured for $\phi_H = 86°$. AGFM (c) and MOKE (d) measurements are also shown. The open symbols give the starting points of the recoil curves.

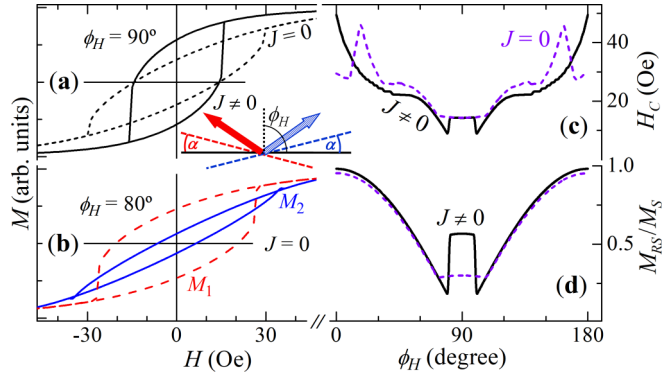

FIG. 5. Model results obtained for two coupled grains with misaligned easy axes with $\alpha = \pm 17.5°$ and $2K/M_S = 50$ Oe. (a) Major loops ($M_1 \equiv M_2$) obtained for $\phi_H = 90°$ using $J = 0$ (dashed line) and $J/K = 0.6$ (solid line). (b) $M_1(H)$ and $M_2(H)$ for $J = 0$ and $\phi_H = 80°$. Angular variations of H_C (c) and M_{RS} (d) for $J = 0$ (dashed lines) and $J/K = 0.6$ (solid lines). The arrows in the schematic depict $\mathbf{M_1}$ and $\mathbf{M_2}$ at remanence.

Apparently, the RCO's intensity (quantified, e.g., through the loop's area or the value of either M_R or H_C) depends on the film's thickness, ϕ_H and H_R. For a particular $\mathbf{H}$ orientation, the intensity of each of the RCO's characteristics, e.g., M_R, attains its extremum for a certain H_R value near the closure field. A recoil curve obtained for $\phi_H = 84°$ for the Co film discussed above (see Fig. 2) is given in Fig. 4(a). Its M_R, H_C, and loop area are 4.4, 5.0, and 2.5 times, respectively, greater than those of the major loop. The gradual RCO's attenuation with H_R after the maximum of M_R is reached is exemplified in Fig. 4(b). Data obtained via AGFM or MOKE at nearly the same configurations, presented in Figs. 4(c) and 4(d), show the same characteristics.

The manifestation of RCO was also investigated in the Ni films. Magnetization data obtained via VSM, AGFM, and MOKE for the 75-nm-thick film are given in Fig. S2 of SM [10], which shows that the phenomenon is clearly observed. The Ta/Ni (20 nm)/Ta film also showed RCO, though rather less expressed as compared with that presented by the Ta/Ni (75 nm)/Ta film. We successfully verified RCO in the Fe film as well; the respective data are shown in Fig. S3 of the SM [10].

We also obtained that RCO is revealed in a rather wide range of ϕ_H. For example, RCO is observed for $65° \leqslant \phi_H \leqslant 115°$ for the Ta/Co (20 nm)/Ta film, and for $50° \leqslant \phi_H \leqslant 130°$ for the Ta/Ni (75 nm)/Ta film, approximately.

Idigoras *et al.* [11,12] have reproduced $M_{RS}(\phi_H)$ very similar to ours by devising a two-grain Stoner-Wohlfarth model that mimics the partial crystalline disorder of a polycrystalline film consisting of pairs of exchange-coupled grains with misaligned anisotropy axes. It has later been used to explain the collapsed hard axis of CoPd thin films with either fourfold or twofold anisotropy [13]. We also adopted this model considering grains with magnetizations $\mathbf{M_1}$ and $\mathbf{M_2}$ with slightly misaligned in-plane anisotropy axes, ea_1 and ea_2, characterized by uniaxial anisotropy constants K_1 and K_2. The misalignment angles between ea_1 and ea_2 with the averaged *EA* are α_1 and α_2 of opposite signs, and the in-plane orientation angles of $\mathbf{M_1}$ and $\mathbf{M_2}$ with respect to *EA* are ϕ_1 and ϕ_2. The grains are exchange coupled, being J the coupling constant. The variable part of the system's free magnetic energy, per unit volume, is

$$\eta = K_1 \sin^2(\phi_1 - \alpha_1) + K_2 \sin^2(\phi_2 - \alpha_2) - J\cos(\phi_1 - \phi_2) - HM_1\cos(\phi_H - \phi_1) - HM_2\cos(\phi_H - \phi_2),$$

where the first two terms correspond to the anisotropy energies, the third one is the exchange-coupling energy, and the two last terms give the respective Zeeman energies. Due to the film geometry and easy axes aligned within the surface plane, the magnetization rotation occurs in the film's plane. Here we simulated complete hysteresis loops employing a previously developed numerical procedure [14–16], thus allowing the identification of the processes leading to the RCO.

It is straightforward to show that the normalized remanent magnetization M_{RS}/M_S for $\phi_H = 90°$, for the simplest case of $\alpha_1 = -\alpha_2 = \alpha$, $M_1 = M_2$, and $K_1 = K_2 = K$, equals $\cos(\frac{\pi}{2} - \frac{1}{2}\arctan\frac{\sin 2\alpha}{\cos 2\alpha - J/K})$. Figure 5(a) shows the respective major loops calculated using $J/K = 0$ and 0.6, while $H_C(\phi_H)$ and $M_{RS}(\phi_H)$ are given in Figs. 5(c) and 5(d). Those calculated for $J \neq 0$ agree qualitatively with the experiment (see Fig. 1). The reversal of $\mathbf{M_1}$ and $\mathbf{M_2}$ is indistinguishable when $\phi_H = 90°$ due to the symmetry of this configuration, no matter the value of J. For ϕ_H close to 90°, however, the angles that $\mathbf{H}$ forms with ea_1 and ea_2 are different so these have distinct anisotropy fields. As seen in Fig. 5(b), where the case of $J = 0$ with $\phi_H = 80°$ is exemplified, $M_1(H)$ and $M_2(H)$ differ significantly, $\mathbf{M_1}$ rotating irreversibly earlier than $\mathbf{M_2}$.

Except for the close vicinity of $\phi_H = 90°$, the exchange coupling results in a single-domain behavior given that the simulated $H_C(\phi_H)$ and $H_R(\phi_H)$ are very similar to those obtained through the Stoner-Wohlfarth model.

A major loop and a recoil curve, simulated with the parameters used in Fig. 5(b) but for $J \neq 0$, are plotted in Fig. 6(a). Both curves are qualitatively very similar to those shown in Figs. 3(b)–3(d). $M_1(H)$ and $M_2(H)$ of the descending branch of the major loop from Fig. 6(a) are given in Fig. 6(b), and

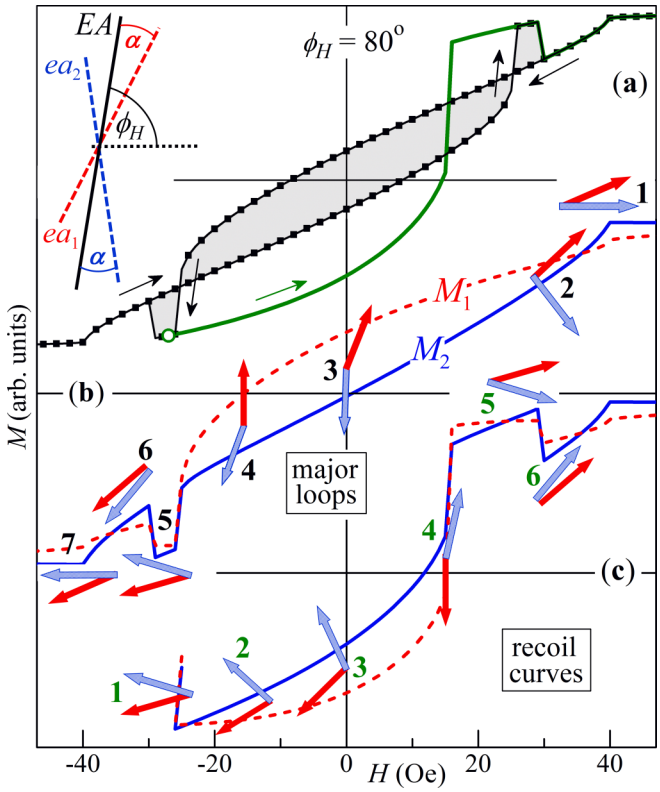

FIG. 6. (a) Major loop (symbols) and a recoil curve (solid line) simulated with the parameters used in Fig. 5(b) but for $J/K = 0.6$. $M_1(H)$ and $M_2(H)$ of the descending branch of the major loop (b) and of the recoil curve (c); the arrows indicate the orientations of $\mathbf{M_1}$ and $\mathbf{M_2}$ at representative sequentially numbered states.

those of the respective recoil curve are shown in Fig. 6(c); the orientations of $\mathbf{M_1}$ and $\mathbf{M_2}$ at selected sequentially numbered states are depicted by arrows. Upon decreasing H from saturation to zero, each of $\mathbf{M_1}$ and $\mathbf{M_2}$ tends to align with the direction of its easy axis closest to the field orientation. For the particular orientations of $\mathbf{H}$, ea_1, and ea_2 [see the schematic in Fig. 6(a)], $\mathbf{M_1}$ and $\mathbf{M_2}$ rotate into opposite directions. At remanence, $\mathbf{M_2}$ and $\mathbf{H}$ are almost perpendicular, leading to a substantial decrease of the system's M_R.

As $\mathbf{H}$ is reversed and its value gradually increased, $\mathbf{M_1}$ and $\mathbf{M_2}$ rotate as normally expected until the irreversible rotation of $\mathbf{M_1}$ which occurs first and at a field a little lower than that of the $J = 0$ case [see Fig. 5(b)]. After this jump, $\mathbf{M_1}$ tries to align with the other direction of ea_1, which is closer to the reversed $\mathbf{H}$; consequently $\mathbf{M_2}$, exchange-coupled to $\mathbf{M_1}$, is "dragged" to switch together. It also tries to align with the closest to $\mathbf{H}$ direction of ea_2 much earlier than would occur if $J = 0$. This direction of ea_2 is rather close to $\mathbf{H}$, so M_2 is prominent. Due to the coupling, $\mathbf{M_1}$ tries to align with $\mathbf{M_2}$ and, consequently, with $\mathbf{H}$. These processes result in the state number 5 in Fig. 6(b) characterized with high values of both M_1 and M_2, responsible for the kink seen just before the closure field of $M(H)$ in Fig. 6(a).

A further increase of H, however, reinforces the Zeeman term of $\mathbf{M_2}$ which overcomes the exchange-coupling one so $\mathbf{M_2}$ is switched back to lie in the vicinity of the other direction of ea_2. From this state, M_2 changes with H following the trend it has before the kink, and M_1 evolves in a manner similar to that seen in Fig. 5(b) for fields higher than that of the irreversible jump of $\mathbf{M_1}$. Finally, at sufficiently high H, $\mathbf{M_2}$ rotates irreversibly to lie between $\mathbf{H}$ and the direction of ea_2 closest to $\mathbf{H}$, and $M(H)$ gradually evolves towards M_S.

The kink in $M(H)$ predicted by our simulations is clearly present in experimental loops [see Figs. 3(b)–3(d) and 4(d)]. Such a behavior has previously been observed though it has remained unexplained [13,17,18].

Let us now unravel the appearance of RCO. The initial state of the recoil curve in Fig. 6(c) is that of state number 5 in Fig. 6(b), the one with the particularly high values of M_1 and M_2. As H is decreased from this frustrated state to zero, the scissorlike magnetization state of $\mathbf{M_1}$ and $\mathbf{M_2}$ slowly changes, resulting in a quite moderate decrease of $M(H)$ and a value of M_R significantly higher than that of the major loop. With the reversion of the field's direction and its gradual increase, a state of practically antiparallel $\mathbf{M_1}$ and $\mathbf{M_2}$ is achieved. In such configuration, the coupling energy is at maximum so a tiny rise of H leads $\mathbf{M_1}$ (the moment with weaker anisotropy) to switch irreversibly. In a manner analogous to that resulting in state 5 of panel (b), $\mathbf{M_2}$ is "dragged" to switch together with $\mathbf{M_1}$ and a reversed state very similar to state 5 of panel (b) is attained, though at a lower field value. For further increase of H, $M(H)$ evolves in a way analogous to the $5 \rightarrow 6 \rightarrow 7$ sequence shown in Fig. 6(b).

One might find a similarity between RCO and exchange bias (EB) [19], i.e., the shift of a hysteresis loop along the H axis resulting from coupling between magnetically stable grains with uncompensated spins and an adjacent softer magnetic phase. A recoil loop presenting RCO can be formally treated as a loop shifted in the direction opposite to that of the higher-anisotropy moment (here, $\mathbf{M_2}$). When $\mathbf{M_2}$ is in the virtually saturated state 1 in Fig. 6(c), it plays the role uncompensated spins do in EB. Along the recoil curve, both $\mathbf{M_1}$ and $\mathbf{M_2}$ follow high-magnetization paths devising a "shifted" loop with H_C of its ascending branch greater than the other. This shift of a loop which lies *outside* the major one must be distinguished from that of a minor loop (confined inside the major loop) resulting from nonsaturation and occasionally misinterpreted as EB [6,7].

By considering proper distributions in size, anisotropy and coupling constants as well as misalignment angles, one should be able to simulate magnetization curves that better reproduce particular experimental data. Although such approach certainly deserves investigation, it is beyond the scope of this work.

One should obtain identical results considering a film that consists of noninteracting polycrystalline grains. Up to a certain field angle, each grain would be in a single-domain magnetic state. During demagnetization from saturation for ϕ_H in the vicinity of 90°, the monodomain would split into two exchange-coupled magnetic domains with slightly misaligned anisotropy axes. Such a hypothesis is in agreement with Scheurer *et al.* [20] that associated the hard-axis collapse with coupled twin-domain pairs with slight lateral misalignment, and also with those of Hamrle *et al.* [21] that observed a domain splitting perpendicular to the collapsed hard axis during demagnetization. The average grain sizes of some of our films that present RCO are, most likely, greater than the

critical size for a stable magnetic monodomain, which seems to support the above conjecture as well.

IV. SUMMARY AND CONCLUSIONS

We report striking magnetization reversal in polycrystalline Co, Fe, and Ni films with uniaxial in-plane magnetic anisotropy, namely, some recoil curves lie entirely outside the major loop. Adopting the model of pairs of exchange-coupled grains with misaligned anisotropy axes, we were able to successfully reproduce all key features of the hysteresis loops including the hard-axis collapse, the recoil loop overshoot, and the kink some major loops present before saturation. We observed RCO for the only three single elements which display room-temperature ferromagnetism, but we believe that it should be found in a variety of polycrystalline thin films with collapsed hard magnetization axes.

ACKNOWLEDGMENTS

J.G. appreciates useful discussions with V. Skumryev, J. E. Schmidt, M. Mikhov, and J. Nogués. The research is partly financed by the Brazilian agencies CNPq (Grants No. 422740/2018-7 and No. 313624/2020-8) and FAPERGS (Grant No. PRONEX 16/0490-0).

[1] G. Bertotti, *Hysteresis in Magnetism* (Academic, San Diego, 1998), p. 17.
[2] J. J. Becker, IEEE Trans. Magn. **9**, 161 (1973); **12**, 965 (1976).
[3] I. D. Mayergoyz, J. Appl. Phys. **57**, 3803 (1985).
[4] J. Geshev, J. Magn. Magn. Mater. **476**, 135 (2018).
[5] R. Skomski and J. M. D. Coey, *Permanent Magnetism* (Institute of Physics, Bristol, 1999), p. 170.
[6] J. Geshev, J. Appl. Phys. **105**, 066108 (2009).
[7] A. Harres, M. Mikhov, V. Skumryev, A. M. H. De Andrade, J. E. Schmidt, and J. Geshev, J. Magn. Magn. Mater. **402**, 76 (2016).
[8] K. Vahaplar, S. Tari, H. Tokuc, and S. Okur, J. Vac. Sci. Technol. B **27**, 2112 (2009).
[9] E. C. Stoner and E. P. Wohlfarth, Philos. Trans. R. Soc. London, Ser. A **240**, 559 (1948).
[10] See Supplemental Material at http://link.aps.org/supplemental/10.1103/PhysRevB.104.054436 for details on the magnetization measurements and three additional figures not included in the original work.
[11] O. Idigoras, A. K. Suszka, P. Vavassori, B. Obry, B. Hillebrands, P. Landeros, and A. Berger, J. Appl. Phys. **115**, 083912 (2014).
[12] O. Idigoras, A. K. Suszka, P. Vavassori, P. Landeros, J. M. Porro, and A. Berger, Phys. Rev. B **84**, 132403 (2011).
[13] M. Sedrpooshan, H. Ahmadvand, D. L. González, and S. van Dijken, Phys. Rev. B **98**, 214444 (2018).
[14] J. Geshev, O. Popov, V. Masheva, and M. Mikhov, J. Magn. Magn. Mater. **92**, 185 (1990).
[15] J. Geshev, A. D. C. Viegas, and J. E. Schmidt, J. Appl. Phys. **84**, 1488 (1998).
[16] A. Harres and J. Geshev, J. Phys.: Condens. Matter **23**, 216003 (2011).
[17] Q.-M. Zhong, A. S. Arrott, B. Heinrich, and Z. Calinski, J. Appl. Phys. **67**, 4448 (1990).
[18] J. A. C. Bland, M. J. Baird, H. T. Leung, A. J. R. Ives, K. D. Mackay, and H. P. Hughes, J. Magn. Magn. Mater. **113**, 178 (1992).
[19] W. H. Meiklejohn and C. P. Bean, Phys. Rev. **102**, 1413 (1956); **105**, 904 (1957).
[20] F. Scheurer, R. Allenspach, P. Xhonneux, and E. Courtens, Phys. Rev. B **48**, 9890 (1993).
[21] J. Hamrle, S. Blomeier, O. Gaier, B. Hillebrands, R. Schäfer, and M. Jourdan, J. Appl. Phys. **100**, 103904 (2006).